Journal of
Materials Chemistry A

Accepted Manuscript

This article can be cited before page numbers have been issued, to do this please use: L. Lu, S. Wang, C. Zhou, Z. shi, H. Zhu, X. Wang, Z. Xin, S. C. Yan and Z. Zou, *J. Mater. Chem. A*, 2018, DOI: 10.1039/C8TA05339A.

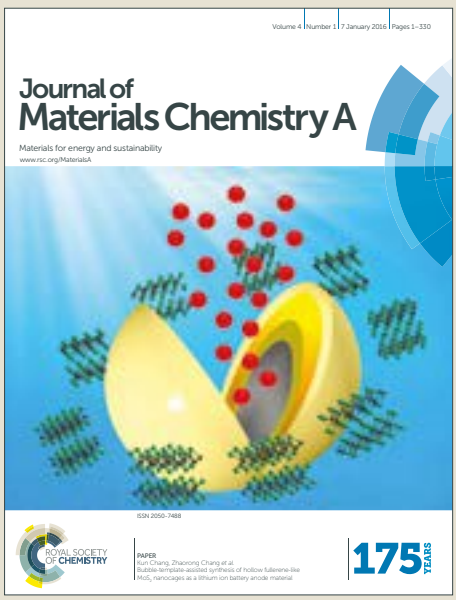

ROYAL SOCIETY OF CHEMISTRY

rsc.li/materials-a

Journal of Materials Chemistry A
View Article Online
DOI: 10.1039/C8TA05339A

Journal Name

ARTICLE

Surface chemistry imposing selective reduction of CO_2 to CO over $Ta_3N_5/LaTiO_2N$ photocatalyst†

Received 00th January 20xx,
Accepted 00th January 20xx

DOI: 10.1039/x0xx00000x

www.rsc.org/

Lei Lu,‡[a] Shaomang Wang,‡[b,c] Chenguang Zhou,‡[a] Zhan Shi,[b] Heng Zhu,[a] Zhenyu Xin,[a] Xiaohui Wang,[a] Shicheng Yan,*[a] and Zhigang Zou[a,b]

Revealing the mechanism of photocatalytic product selectivity will provide valuable guidance on developing novel catalysts and reaction pathways. Here, the roles of surface chemistry on product generation are well demonstrated over $LaTiO_2N$, Ta_3N_5, and their hybrids, respectively with dominant (002) and (020) facet. The photocatalytic test results show that the CO_2 is reduced to CH_4 and CO over $LaTiO_2N$ and Ta_3N_5 photocatalysts, respectively. The CO_2 reduction over $LaTiO_2N$ and Ta_3N_5 follows the possible reaction pathway *via* $CO_2 \rightarrow COOH^* \rightarrow CO \rightarrow CH_x^* \rightarrow CH_4$, as proposed by the detected intermediates. The product selectivity is dependent on the ability of capturing CO onto photocatalyst surface, probably related to electronegativity of the adsorption sites. The strongly adsorbed CO on $LaTiO_2N$ surface favors the subsequent hydrogenation reaction to generate CH_4, while the weak CO adsorption on Ta_3N_5 induces the CO as a main product of CO_2 reduction, as well demonstrated by theoretical calculation. Such product selectivity is mainly related to the surface chemistry and is independent on the surface charge concentration of photocatalyst. Our results provide a progressive understanding of the selective product formation during the photocatalytic CO_2 reduction.

Introduction

Reduction of CO_2 over semiconductor photocatalyst is recognized to be a potential solution to achieve the recycling of carbon source.[1-3] Under irradiation, driven by photogenerated electrons of semi-conductor, CO_2 can be reduced into various value-added fuels, such as CO, HCO_2H, HCOH, CH_3OH, or CH_4, in the presence of protons that are commonly provided from H_2O splitting by photogenerated hole oxidation.[4] To date, much concern has been focused on improving the efficiency of the solar-driven CO_2 conversion. However, the product selectivity is still not well understood.

In theory, the formation of reduced products depends on the number of transferring electrons and protons, typically two-electron process for CO and eight-electron requirement for CH_4.[5] Actually, among the reported gaseous CO_2 reductions, the CO and CH_4 are usually detected as the main product over different photocatalysts.[6-9] For instance, the TiO_2 or C_3N_4 without additional decoration presented excellent CO selectivity,[6,7] while the selective CH_4 formation was observed over $ZnGa_2O_4$ and Zn_2GeO_4.[8,9] Surface modification including introducing basic sites or loading cocatalysts could induce the CH_4 as main product over TiO_2 or C_3N_4.[10-14] Meanwhile, exposing the (110) facet of Zn_2GeO_4 produced the CO as main product.[15] The similar facet dependence of reduced products was also demonstrated on TiO_2 and $BiVO_4$.[16-18] These results indicate that the product selectivity of CO_2 reduction is strongly related to surface chemistry of photocatalyst, since the two half-reactions of H_2O oxidation and CO_2 reduction both take place on the photocatalyst surface.

In the previous reports, accompanied by the increase of electron concentration on the surface of photocatalysts by loading cocatalysts, effectively promoted CH_4 formation was observed. Therefore, the product selectivity was considered to be dependent on the charge concentration. Such a standpoint was well demonstrated by forming heterojunction or metal-semiconductor junction to enhance the charge separation efficiency.[10,11,19-22] Typically, the Pt modification on TiO_2 accelerated the formation of CH_4.[10,11] However, different reduced products could be detected when using the different electrocatalysts. Correspondingly, the Ag and Au are beneficial for CO formation,[23,24] while Cu commonly shows a combination of hydrocarbons.[25] This fact means that, in addition to electron concentration, the surface chemistry of catalysts may also play an important role on the product selectivity. Indeed, the difference in CO_2 activation on the surface of various metals or oxides, which determines the reaction pathway and product selectivity, has been investigated in thermocatalysis of CO_2 conversion.[26] Actually, for explaining the product selectivity of photocatalytic CO_2 reduction, theoretical calculations that using the TiO_2 as a material model have proposed two reaction pathways,

[a] Eco-materials and Renewable Energy Research Center (ERERC), National Laboratory of Solid State Microstructures, Collaborative Innovation Center of Advanced Microstructures, College of Engineering and Applied Sciences, Nanjing University, 210093 (P. R. China)
[b] Jiangsu Province Key Laboratory for Nanotechnology, School of Physics, Nanjing University, Nanjing, Jiangsu 210093 (P. R. China)
[c] School of Environment and Safety Engineering, Changzhou University, Changzhou 213164 (P. R. China)
E-mail: yscfei@nju.edu.cn
†Electronic Supplementary Information (ESI) available. See DOI: 10.1039/x0xx00000x
‡These authors contributed equally to this work.

View Article Online
DOI: 10.1039/C8TA05339A

respectively calling fast-hydrogenation (FH) pathway (CO_2 → HCOOH/CO → CH_2O → CH_3OH → CH_4) and fast deoxygenation (FdO) pathway (CO_2 → CO → C^* → CH_3^* → CH_4).[5,27] However, it is necessary to further understand the effect of surface chemistry on product selectivity, due to that the molecule activation, reaction pathway, and product formation are highly sensitive to the surface properties of catalysts.

Here, to identify the importance of surface chemistry in product formation of the photocatalytic CO_2 reduction, photocatalysts of porous $LaTiO_2N$ plates with exposure of (002) facet, Ta_3N_5 nanorods with exposure of (020) facet, and the corresponding $Ta_3N_5/LaTiO_2N$ composite were prepared by respectively nitriding $La_2Ti_2O_7$ plates, $KTaO_3$ microcubes, and their mixtures under flowing NH_3. The photocatalytic CO_2 reduction tests showed that the CO_2 was, respectively, reduced into CH_4 and CO over $LaTiO_2N$ and Ta_3N_5. Proposed by the detected intermediates, the CO_2 reduction over $LaTiO_2N$ and Ta_3N_5 possibly followed the reaction pathway of CO_2 → $COOH^*$ → CO → CH_x^* → CH_4. Theoretical calculation showed that the product selectivity was dependent on the ability of capturing CO onto photocatalyst surface, probably resulting from the different electronegativity of adsorption sites. The strongly adsorbed CO on $LaTiO_2N$ surface favored the subsequent hydrogenation reaction to generate CH_4. However, the weak CO adsorption on Ta_3N_5 induced the CO as a main product of CO_2 reduction. Indeed, when using CO as carbon source, the $LaTiO_2N$ could rapidly convert the CO into CH_4, while the Ta_3N_5 showed a much lower conversion efficiency. Moreover, all the $Ta_3N_5/LaTiO_2N$ samples, where CO_2 reduction took place on Ta_3N_5 surface, evolved CO as main product during the CO_2 conversion. These results confirmed that such product selectivity was mainly related to the surface chemistry and was independent on the surface charge concentration of photocatalyst, providing us a progressive understanding of the selective product formation for the photocatalytic CO_2 reduction.

Experimental Section

Synthesis of $La_2Ti_2O_7$ and $KTaO_3$ precursors: The solid $La_2Ti_2O_7$ powder was synthesized by a typical flux-assisted growth method. Simply, a stoichiometric mixture of La_2O_3 and TiO_2 was thoroughly mixed with NaCl and KCl compounds (NaCl: KCl=1:1), in which the $La_2Ti_2O_7$ product accounts for 5% mole ratio. The resulting mixtures were heated to 1273 K with a raise rate of 100 K/h and held at this temperature for 10 h. After a cooling process to 973 K at a rate of 50 K/h, it was cooled to room temperature naturally. The $KTaO_3$ microcubes were prepared by a hydrothermal reaction. Typically, Ta_2O_5 powder (0.4 g) was added to KOH solution (30 mL, 1 M). After ultrasonic dispersion, the resultant suspension was poured into a 50 mL Teflon vessel and heated to 433 K for 12 h. Notably, both the obtained white powders of $La_2Ti_2O_7$ and $KTaO_3$ were separated by deionized water washing and dried in an oven at 353 K overnight.

Preparation of $Ta_3N_5/LaTiO_2N$ photocatalyst: The $LaTiO_2N$ and Ta_3N_5 were prepared by respectively nitriding the as-prepared $La_2Ti_2O_7$ and $KTaO_3$ precursors (about 0.2 g for each run) under 200 mL/min flowing NH_3 at 1223 K for 18 h at a rate of 10 K/min, followed by a natural cooling process to room temperature. To obtain the heterojunction of $Ta_3N_5/LaTiO_2N$, the $La_2Ti_2O_7$ and $KTaO_3$ precursors were mixed intensively, and the same nitridation process was carried out. For comparison, $Ta_3N_5/LaTiO_2N$ samples with different Ta_3N_5 ratio were prepared, and the ratio of Ta_3N_5 to $LaTiO_2N$ was achieved by changing the amount of $KTaO_3$. All the obtained products were washed with deionized water, and dried in a vacuum oven.

Photoreduction CO_2 testing: The gas phase photocatalytic reduction of CO_2 was tested in a glass reactor with an area of 4.2 cm^2 using H_2O as reducing agent, and photocatalyst (40 mg) was uniformly dispersed. The light source was a 300 W Xenon arc lamp fitted with a cutoff filter ($\lambda > 420$ nm). The volume of the reaction chamber was about 230 mL. Before the irradiation, the reaction system was vacuumed several times, and then high-purity gas of compressed CO_2 (purity 99.999%) was introduced into the reaction chamber to achieve an ambient pressure. Subsequently, deionized water (0.4 mL) was injected into the chamber as reactant. Prior to irradiation, the adsorption process was held for 2 h. During the reaction, 1 mL gas was extracted by a sampling needle from the chamber at given intervals for subsequent concentration analysis. The carbon-based products were quantified by a gas chromatography (GC-2014, Shimadzu Corp., Japan) with flame ionization detector (FID).

Materials characterizations: The crystal phases were determined by powder X-ray diffraction (XRD, Rigaku Ultima III, Japan) operated at 20 kV and 40 mA with Cu-Kα radiation. The surface morphology was observed by scanning electron microscopy (SEM, FEI Nova Nano SEM 230, USA). High-solution lattice images and selected area electron diffraction (SAED) patterns was obtained by transmission electron microscopy (TEM, FEI Tecnai G2 F30 S-Twin, USA) operated at 200 kV. Diffused reflectance spectrum was scanned by a UV-vis spectrophotometer (UV-2500, Shimadzu Co., Japan) and transformed into absorption spectrum with Kubelka-Munk relationship. The specific surface area was measured from nitrogen (N_2) adsorption-desorption isotherm at 77 K by an automatic surface area analyzer (Micromeritics Tristar-3000, USA) after the samples had been dehydrated at 423 K for 2 h in the flowing N_2. The CO_2 adsorption was measured by the applied BET method at 273 K. The surface chemical species was investigated by X-ray photoelectron spectroscopy (XPS) on PHI5000 Versa Probe (ULVAC-PHI, Japan) with monochromatized Al Kα X-ray radiation (1486.6 eV). The energy resolution of the electrons analyzed by the hemi-spherical mirror analyzer is about 0.2 eV. The C 1s core level at 284.6 eV was taken as an internal reference to correct the shift of the binding energies. The room temperature photoluminescence (PL) spectra were acquired using an objective-scanning confocal microscope system, in which the samples were excited through an oil-immersion objective lens (Olympus, SR-ASZ-0103, 150) using a 40 mW pulsed laser (488 nm). The flat band positions of the Ta_3N_5 and $LaTiO_2N$ were estimated by Mott-Schottky measurement, which was carried out using a Princeton Applied Research PARSTAT 2273, using 0.5 M Na_2SO_4 aqueous solution as electrolyte with a pH value of 7. The frequency was 500, 1000, and 2000 Hz.

Computational calculations: The calculations of adsorption

View Article Online
DOI: 10.1039/C8TA05339A

energy were conducted through the Cambridge Serial Total Energy Package (CSTEP) code. The general gradient approximation with Perdew-Bueke-Ernzerh (PBE) functional was employed to describe the exchange–correlation effects. The attractive energy between nuclear and electrons was calculated via ultrasoft pseudopotential. The convergence threshold of geometric optimization was set at 2.0 $\times 10^{-5}$ eV per atom for total energy, 0.05 eV $Å^{-1}$ for maximum force, 0.1 GPa for stress, and 0.002 Å for maximum displacement. The crystal structure of Ta_3N_5 (020) was built including 9 atoms of Ta, 15 atoms of N, and lattice parameter was a = 10.3 Å, b = 3.9 Å, c = 17.0 Å and α = β = γ = 90°. The crystal structure of $LaTiO_2N$ (002) contained 3 atoms of La, 3 atoms of Ti, 6 atoms of O, and 3 atoms of N, and lattice parameter was a = 5.6 Å, b = 7.9 Å, c = 16.5 Å, α = β = 90° and γ = 89.9°.

Results and Discussion

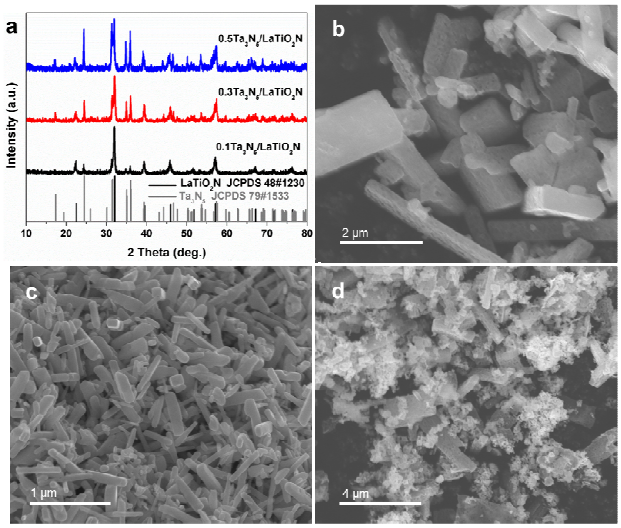

Fig. 1 (a) XRD patterns for the as-prepared $xTa_3N_5/LaTiO_2N$ (x = 0.1, 0.3, and 0.5) samples. SEM images of (b) $LaTiO_2N$, (c) Ta_3N_5, and (d) $0.3Ta_3N_5/LaTiO_2N$.

To obtain our designed photocatalysts, precursors of $La_2Ti_2O_7$ and $KTaO_3$ were first prepared. $La_2Ti_2O_7$ was prepared by heating stoichiometric mixture of La_2O_3 and TiO_2 in a molten salt of NaCl and KCl at 1273 K. $KTaO_3$ was synthesized by a hydrothermal method at 433 K using Ta_2O_5 and KOH as reagents. X-ray diffraction (XRD) patterns showed that the as-prepared $La_2Ti_2O_7$ (JCPDS No. 70-1690) and $KTaO_3$ (JCPDS No. 77-0198) were both crystallized in single phase with orthorhombic structure (**Fig. S1a** and **S1b, ESI**†). Scanning electron microscope (SEM, **Fig. S1c** and **S1d, ESI**†) images showed the plate-like $La_2Ti_2O_7$ (0.4-0.6 μm in thickness, 1.5-1.7 μm in width, and 3.5-4 μm in length) and $KTaO_3$ microcubes (0.2-0.3 μm in side length). After heating the mixtures of $La_2Ti_2O_7$ and $KTaO_3$ under flowing NH_3 at 1223 K, the XRD peaks (**Fig. 1a**) of the products were well indexed to mixtures of Ta_3N_5 (JCPDS No. 79-1533) and $LaTiO_2N$ (JCPDS No. 48-1230). This evidence indicated that both $La_2Ti_2O_7$ and $KTaO_3$ could be completely converted into $LaTiO_2N$ and Ta_3N_5. Indeed, pure $LaTiO_2N$ and Ta_3N_5 were obtained by directly nitriding their precursors (**Fig. S1a** and **S1b, ESI**†). The obtained hybrids were denoted as $xTa_3N_5/LaTiO_2N$, where the x represented the mole ratio between Ta_3N_5 and $LaTiO_2N$. Accordingly, with increasing the ratio of $KTaO_3/La_2Ti_2O_7$, continuously enhanced intensity of Ta_3N_5 diffraction peaks was observed.

The SEM image of the obtained $LaTiO_2N$ showed a porous structure with apparent profile and size of $La_2Ti_2O_7$ precursor (**Fig. 1b**). However, great morphology change was observed for phase transformation from $KTaO_3$ microcubes to Ta_3N_5, which was shaped in nanorods with particle size of 60-80 nm in width and 0.3-0.5 μm in length (**Fig. 1c**). This fact indicated that the formation of $LaTiO_2N$ driven by nitriding $La_2Ti_2O_7$ was pseudomorphic and topotactic.[28] The particles with porous structure were resulted from the volume shrinkage during replacing the three O atoms by two N atoms.[28] In contrast, a recrystallization-growth process maybe occur during the Ta_3N_5 formation due to the potassium removal from $KTaO_3$, thus destroying the profile of precursor. For the composite materials, taken $0.3Ta_3N_5/LaTiO_2N$ as an example, the typical morphologies of $LaTiO_2N$ porous plates and Ta_3N_5 nanorods were also observed (**Fig. 1d**), in which the Ta_3N_5 nanorods were uniformly distributed around $LaTiO_2N$ plates. This indicated that the one-step nitriding did not change their morphologies.

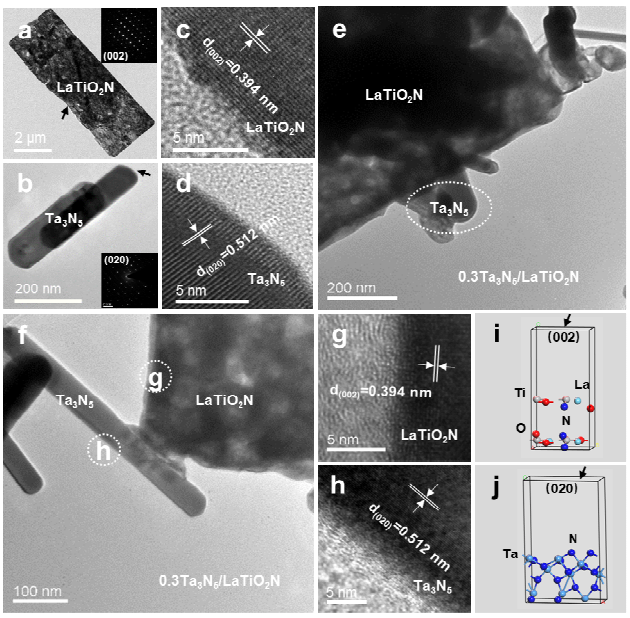

Fig. 2 TEM images of (a) $LaTiO_2N$ and (b) Ta_3N_5. The inset shows the corresponding SAED images. HR-TEM images of (c) $LaTiO_2N$ and (d) Ta_3N_5. (e) and (f) TEM images of $0.3Ta_3N_5/LaTiO_2N$. HR-TEM images of (g) $LaTiO_2N$ and (h) Ta_3N_5 in $0.3Ta_3N_5/LaTiO_2N$. Side view of surface structure model for (i) (002) facet of $LaTiO_2N$ and (j) (020) facet of Ta_3N_5.

Observations of the transmission electron microscope (TEM) further confirmed the typical morphologies of $LaTiO_2N$ porous plate and Ta_3N_5 nanorod (**Fig. 2a** and **2b**). The corresponding selected area electron diffraction (SAED) patterns well demonstrated the single-crystal nature of the porous $LaTiO_2N$ sheets and Ta_3N_5

View Article Online
DOI: 10.1039/C8TA05339A

nanorods. As shown in high-resolution TEM (HR-TEM) lattice images (**Fig. 2c** and **2d**), the measured lattice spacing of 0.394 and 0.512 nm were, respectively, assigned to (002) and (020) plane of the orthorhombic $LaTiO_2N$ and Ta_3N_5. Apparently, both the (002) facet in $LaTiO_2N$ and (020) facet in Ta_3N_5 were highly exposed. The representative TEM images of $0.3Ta_3N_5/LaTiO_2N$ were shown in **Fig. 2e** and **2f**. Due to the significant difference in morphology and shape size, $LaTiO_2N$ and Ta_3N_5 could be easily identified. Intimate contact at the interface was found, well confirming the formation of $Ta_3N_5/LaTiO_2N$ heterojunction. Moreover, the (002) facet of $LaTiO_2N$ and (020) facet of Ta_3N_5 were observed in the composite of $LaTiO_2N$ and Ta_3N_5 (**Fig. 2g** and **2h**), indicating that they followed the same growth mechanism during the two synthetic processes. The calculated surface structure model showed that the (002) facet of $LaTiO_2N$ was composed of equal anions and cations, respectively involving one La atom, two Ti atoms, one N atom, and two O atoms (**Fig. 2i**). In contrast, the (020) facet in Ta_3N_5 was dominated by N atoms, and Ta atoms located at the sublayer (**Fig. 2j**). Commonly, the metal sites in catalysts are demonstrated to be active sites for CO_2 adsorption.[29] This result suggested that the exposed (020) facet of Ta_3N_5 was possibly unfavorable for capturing CO_2 or the intermediates.

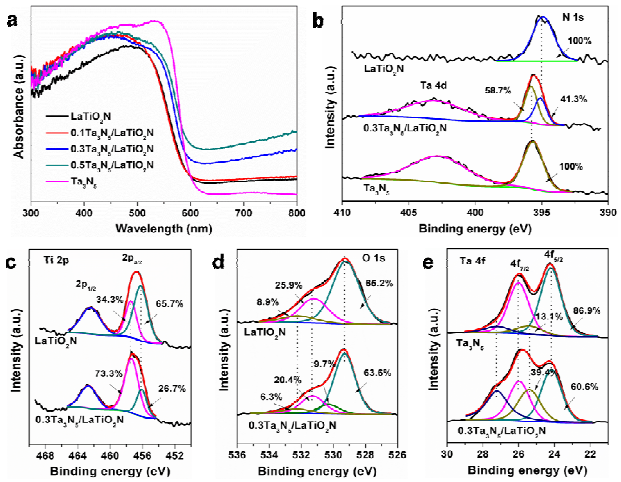

Fig. 3 (a) UV-vis absorption spectra for $LaTiO_2N$, Ta_3N_5, and $xTa_3N_5/LaTiO_2N$ (x = 0.1, 0.3, and 0.5) samples. (b) N 1s XPS spectra for $LaTiO_2N$, Ta_3N_5, and $0.3Ta_3N_5/LaTiO_2N$. (c) Ti 2p and (d) O 1s XPS spectra for $LaTiO_2N$ and $0.3Ta_3N_5/LaTiO_2N$. (e) Ta 4f XPS spectra for Ta_3N_5 and $0.3Ta_3N_5/LaTiO_2N$.

Fig. 3a showed the ultraviolet-visible (UV-vis) absorption spectra. All the samples exhibited a similar visible light absorption up to 600 nm. Compared with the $LaTiO_2N$, gradual increase in absorbance was found for the $Ta_3N_5/LaTiO_2N$ composite with increasing the content of Ta_3N_5. This fact should be a result of higher absorption ability for Ta_3N_5 than $LaTiO_2N$ in the wavelength range from UV region to 600 nm. Interestingly, for the composite samples, obvious upward absorption trail in the wavelength above 600 nm could be observed, especially for the $0.5Ta_3N_5/LaTiO_2N$ sample. Usually, the absorption trail was strongly associated with the light absorption process of defect states.[30-33] It has been widely reported that some defects, such as reduced Ta species, and N or O vacancies,[34-36] could be introduced into the crystal lattice during high-temperature heating process. To exclude the possibility of element doping, Ta-doped $LaTiO_2N$ was prepared by nitriding Ta-doped $La_2Ti_2O_7$. XRD analysis showed that (112) plane of $LaTiO_2N$ shifted to smaller angle (**Fig. S2a, ESI†**), due to the slight larger ionic radius of Ta^{5+} (64 pm) than Ti^{4+} (61 pm), thus confirming that the Ta was successfully incorporated into the lattice of $LaTiO_2N$. Compared with the $LaTiO_2N$, about 10 nm blue-shift of the UV-vis absorption curve and absent absorption trail were found for Ta-doped $LaTiO_2N$ (**Fig. S2b, ESI†**). This evidence meant that, during formation of $Ta_3N_5/LaTiO_2N$ composite, no doping effects were involved. Indeed, XRD peak without position shift was observed in the $Ta_3N_5/LaTiO_2N$ composite (**Fig. S2c, ESI†**), further confirming that no element doping occurred. None absorption trail was also observed in the physically mixed Ta_3N_5+$LaTiO_2N$ sample (**Fig. S3a, ESI†**), suggesting that the increased defect absorption may relate to the strong interaction between Ta_3N_5 and $LaTiO_2N$ due to their compact contact.

To check the interactions between Ta_3N_5 and $LaTiO_2N$, X-ray photoelectron spectroscopy (XPS) analysis was carried out. As can be seen, N 1s XPS for the $0.3Ta_3N_5/LaTiO_2N$ photocatalyst can be deconvoluted into two peaks at 395.6 and 394.9 eV (**Fig. 3b**), respectively assigned to lattice N in Ta_3N_5 and $LaTiO_2N$,[19,30] well demonstrating the composite materials. The binding energy difference was resulted from slightly smaller electronegativity for Ti (3.45 eV) than Ta (4.11 eV). For the single $LaTiO_2N$, Ti 2p XPS spectrum was fitted for Ti^{4+} at 457.8 eV and for Ti^{3+} at 456.7 eV (**Fig. 3c**).[36,37] The Ti^{3+} species in the $LaTiO_2N$ was resulted from the reduction of Ti^{4+} by NH_3 during the nitridation process.[30] The amount of Ti^{3+} species obviously decreased with the formation of $Ta_3N_5/LaTiO_2N$ composite. This fact suggested that the compact contact between Ta_3N_5 and $LaTiO_2N$ could stabilize the lattice Ti^{4+} under NH_3, thus decreasing the Ti^{3+} defect.

For charge balance, the oxygen vacancy and Ti^{3+} species were usually coexisted in the $LaTiO_2N$ or TiO_2.[30,38-41] Usually, the O 1s XPS peak at 531.2 eV was attributed to lattice oxygen atoms near the oxygen vacancy.[30,42] Compared with the $LaTiO_2N$, the $0.3Ta_3N_5/LaTiO_2N$ showed lower oxygen vacancy concentration. This fact further suggested that the compactly contacting Ta_3N_5 with $LaTiO_2N$ was beneficial to stabilize the Ti^{4+} in the lattice of $LaTiO_2N$. The XPS peaks at 529.2 and 532.2 eV were respectively assigned to Ti-O-Ti lattice oxygen and surface adsorbed oxygen species (**Fig. 3d**).[30,43] Notably, for $0.3Ta_3N_5/LaTiO_2N$, one additional peak at 530.2 eV was assigned to TaO_x species in Ta_3N_5.[44] The Ta 4f XPS spectra for both Ta_3N_5 and $0.3Ta_3N_5/LaTiO_2N$ sample were deconvoluted into four peaks: 24.2 eV for Ta 4f 7/2 and 26.0 eV for Ta 4f 5/2 in Ta_3N_5, and 25.4 eV for Ta 4f 7/2 and 27.2 eV for Ta 4f 5/2 in TaO_x species (**Fig. 3e**).[44,45] Obviously, the $0.3Ta_3N_5/LaTiO_2N$ showed higher amount of TaO_x species (39.4%) than the Ta_3N_5 (13.1%). No obvious binding energy difference was observed in La 3d XPS spectra for both the $LaTiO_2N$ and $0.3Ta_3N_5/LaTiO_2N$ (**Fig. S3b, ESI†**), indicating their almost identical surface chemistry for La element. After forming $Ta_3N_5/LaTiO_2N$ composite, the decreased Ti^{3+} species in $LaTiO_2N$ and the increased TaO_x species in Ta_3N_5 maybe suggest that the surface chemistry environment change was

View Article Online
DOI: 10.1039/C8TA05339A

a result of the strong interaction between Ta and Ti. This was comprehensible that after the compact contact, Ti would donate electrons to Ta due to the lower electronegativity for Ti than Ta, thus causing the decreased content of Ti^{3+} and the increased content of TaO_x species. The increased TaO_x defects may be responsible for the increased trail absorption of the $Ta_3N_5/LaTiO_2N$ composite (**Fig. 3a**).

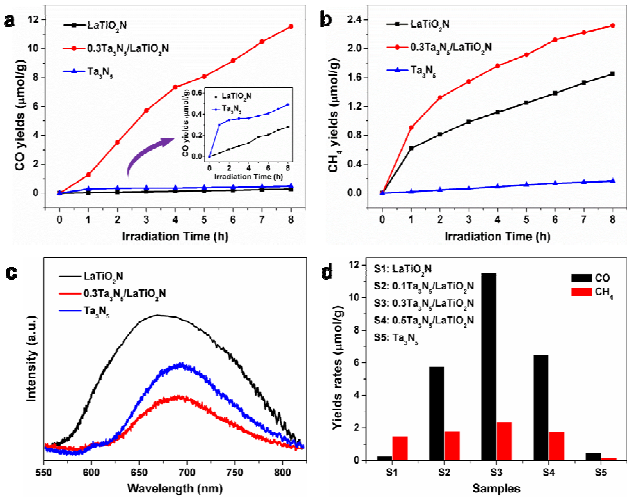

Fig. 4 (a) CO and (b) CH_4 generation, and (c) PL spectra for $LaTiO_2N$, $0.3Ta_3N_5/LaTiO_2N$, and Ta_3N_5. (d) Product generation for $LaTiO_2N$, Ta_3N_5, and x $Ta_3N_5/LaTiO_2N$ (x = 0.1, 0.3, and 0.5). The inset in Fig. 4a shows the enlarged view of CO yields for $LaTiO_2N$ and Ta_3N_5.

The photocatalytic CO_2 reduction tests were carried out over the as-prepared $LaTiO_2N$ porous plates, Ta_3N_5 nanorods, and $Ta_3N_5/LaTiO_2N$ samples under irradiation of visible light ($\lambda \geq 420$ nm) using H_2O as reducing agent. The typical time-course curves of photocatalytic CO_2 reduction were shown in **Fig. 4a** and **4b**. The CO and CH_4 were evolved only under irradiation and their yields increased with prolonging the irradiation time. This result well demonstrated the formation of CO and CH_4 originating from CO_2 photoreduction. Compared with the $LaTiO_2N$ or Ta_3N_5, the $0.3Ta_3N_5/LaTiO_2N$ sample showed much higher CH_4 and CO evolution. As observed by TEM, a compact contact may induce the formation of heterojunction of $LaTiO_2N$ and Ta_3N_5. The Mott-Schottky measurement and UV-vis absorption spectra revealed that the relative conduction band (CB, -0.218 eV) and valence band (VB, +1.902 eV) levels of Ta_3N_5 were, respectively, slightly positive than the CB (-0.332 eV) and VB (+1.768 eV) of $LaTiO_2N$. This fact meant that a typical type-□ heterojunction was formed between $LaTiO_2N$ and Ta_3N_5 (**Fig. S4, ESI†**). The space-charge region electric field, which would contribute to the increased performance in CO_2 reduction, was built at their interface as a result of charge carries diffusion.[46] Under irradiation, this electric field can direct the flow of electrons and holes to different semiconductors, thus resulting in efficient charge separation and low recombination. Indeed, much lower photoluminescence (PL) intensity was observed for the sample of $0.3Ta_3N_5/LaTiO_2N$ by comparing with the $LaTiO_2N$ or Ta_3N_5 (**Fig. 4c**), well demonstrating the decreased recombination of electrons and holes. As expected, the content of Ta_3N_5 played important effects on the CO_2 reduction performance for the $Ta_3N_5/LaTiO_2N$ systems. Typically, with increasing the content of Ta_3N_5, volcano-type distributions of the CH_4 and CO yields were revealed (**Fig. 4d**). And, the $0.3Ta_3N_5/LaTiO_2N$ sample exhibited the highest CH_4 and CO generation rates to be 2.32 and 11.53 μmol/g, respectively. For the $xTa_3N_5/LaTiO_2N$ composite, when $x < 0.3$, the gradually increased CO_2 conversion rate can be attributed to the increased space charge region by forming heterojunction between Ta_3N_5 and $LaTiO_2N$, thus promoting the charge separation and improving the CO_2 reduction. When $x > 0.3$, the decreased CO_2 conversion rate was probably due to the increased TaO_x species on Ta_3N_5, as demonstrated by UV-vis and XPS analysis. The earlier theoretical calculations showed that the Ta^{4+} defect in Ta_3N_5 was the recombination center of electron-hole pairs, thus decreasing the photocatalytic efficiency.[47] All the $Ta_3N_5/LaTiO_2N$ samples showed evidently faster CO_2 reduction rate than the $LaTiO_2N$ or Ta_3N_5, confirming the contribution of $Ta_3N_5/LaTiO_2N$ heterojunction structure.

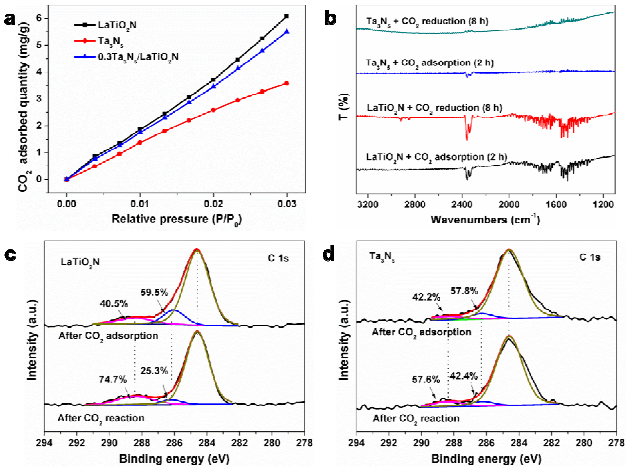

Fig. 5 (a) CO_2 adsorption isotherms for $LaTiO_2N$, Ta_3N_5, and $0.3Ta_3N_5/LaTiO_2N$ samples. (b). FT-IR spectra for $LaTiO_2N$ and Ta_3N_5 after CO_2 adsorption and reduction. C 1s XPS analysis of (c) $LaTiO_2N$ and (d) Ta_3N_5 after CO_2 adsorption and photocatalytic reaction.

After irradiation for 8 h (**Fig. 4d**), the total evolved CH_4 and CO were 1.61 and 0.28 μmol/g for $LaTiO_2N$ and 0.20 and 0.49 μmol/g for Ta_3N_5, respectively. This result indicated that CH_4 and CO were the main product over $LaTiO_2N$ and Ta_3N_5, respectively. The CH_4/CO mole ratio was 5.75 for $LaTiO_2N$ and 0.41 for Ta_3N_5, confirming their different product selectivity for CO_2 reduction. In general, the product selectivity was controlled by the reagent concentration and molecule activation. Indeed, for the CO_2 conversion, it was proposed that CO generation occurred at a low CO_2 reaction rate resulting from the insufficient electrons.[10,11] In our case, the Ta_3N_5 with CO selectivity indeed showed obviously lower CO_2 reduction efficiency than $LaTiO_2N$. However, a lower charge recombination for Ta_3N_5 than $LaTiO_2N$ was verified by PL results (**Fig. 4c**). This fact probably suggested that electron concentration was not mainly responsible for the CO selectivity of Ta_3N_5. As demonstrated in XPS

View Article Online
DOI: 10.1039/C8TA05339A

results, the oxygen vacancies were inevitably generated in the $LaTiO_2N$, which usually served as an important electron transfer route to improve the charge separation efficiency.[30,43] Passivating oxygen vacancies by heating the $LaTiO_2N$ at 353 K under air, the PL intensity evidently increased when prolonged the heat time from 12 h to 24 h (**Fig. S5a, ESI†**), indicating that the oxygen vacancies were indeed responsible for charge separation. Obviously, passivating the oxygen vacancies induced the decrease in CO_2 reduction activity of $LaTiO_2N$, due to the increased charge recombination (**Fig. S5b, ESI†**). And, the CH_4/CO mole ratio decreased from 5.75 for fresh $LaTiO_2N$, to 2.2 for passivating $LaTiO_2N$ for 12 h, and to 1.8 for passivating $LaTiO_2N$ for 24 h. Although the CO yield was increased, the CH_4 was still the main product, implying that the product selectivity was not completely attributed to the charge concentration change. Hence, for the $LaTiO_2N$ or Ta_3N_5, a possible conclusion could be drawn that the surface chemistry of the photocatalyst played a decisive role on the selective product generation rather than the surface electron density. The increased CH_4 and CO yields verified that the charge separation efficiency was evidently improved in the $Ta_3N_5/LaTiO_2N$ heterojunction. Significantly increased CO product selectivity with CH_4/CO mole ratio of 0.2 was achieved by the $0.3Ta_3N_5/LaTiO_2N$ heterojunction, further demonstrating that evolved products were possibly dependent on the surface chemistry, in spite of the improved photocatalytic activity due to the promoted charge separation. Similarly, the *Z*-scheme α-Fe_2O_3/g-C_3N_4 with increased electron concentration only enhanced the CO_2 reduction performance, still presenting the CO product selectivity as the g-C_3N_4.[7]

It was reported that changing the surface chemistry of TiO_2 by doping could change the main product from CO to CH_4.[48] Increasing the NH_3 flow amount from 200 to 500 mL/min, the content of TaO_x species in Ta_3N_5 was decreased from the 13% to 9.3%, as demonstrated by XPS analysis (**Fig. S6a, ESI†**). Correspondingly, the CH_4/CO mole ratio slightly decreased from 0.41 to 0.34, although the CO_2 reduction activity increased approximately two fold due to the decrease of TaO_x as recombination centers (**Fig. S6b, ESI†**). This evidence indicated that the TaO_x species played little effects on the product selectivity of Ta_3N_5. CO_2 adsorption and activation have been demonstrated to be pivotal factors to affect photocatalytic CO_2 reduction.[7,8,30] Brunauer-Emmett-Teller (BET) tests revealed the nearly same BET surface areas for the as-prepared $LaTiO_2N$ (26.49 m^2/g), Ta_3N_5 (23.56 m^2/g), and $0.3Ta_3N_5/LaTiO_2N$ (20.81m^2/g) (**Fig. S6c, ESI†**). Interestingly, the CO_2 adsorption tests (**Fig. 5a**) showed that the maximal adsorption amount of CO_2 on the surface of Ta_3N_5 (3.58 mg/g) was obviously lower than $LaTiO_2N$ (6.08 mg/g) and $0.3Ta_3N_5/LaTiO_2N$ (5.51 mg/g), indicating a stronger CO_2 capture ability for the $LaTiO_2N$-contianing samples than Ta_3N_5. A similar result was obtained by normalizing their CO_2 adsorption quantity with BET surface area to be 0.23 mg/m^2 for $LaTiO_2N$, 0.15 mg/m^2 for Ta_3N_5, and 0.27 mg/m^2 for $0.3Ta_3N_5/LaTiO_2N$, respectively. The higher CO_2 adsorption ability for $LaTiO_2N$-contianing samples was possibly attributed to the porous structure that helped to enhance the molecule adsorption. The $0.3Ta_3N_5/LaTiO_2N$ with strong adsorption of CO_2 exhibited the higher CO selectivity, similar to the Ta_3N_5 with weak adsorption of CO_2, suggesting that the product selectivity could not be completely attributed to the CO_2 molecule adsorption.

Semi-qualitative Fourier transform infrared (FT-IR) spectroscopy analysis was carried out on the $LaTiO_2N$ and Ta_3N_5. After 2 h CO_2 adsorption-desorption equilibrium under dark condition, the $LaTiO_2N$ and Ta_3N_5 exhibited the nearly similar FT-IR bands (**Fig. 5b**). A band at 2347 cm^{-1} was assigned to linearly adsorbed CO_2.[30] The band from 1850 cm^{-1} to 1610 cm^{-1} was attributed to the asymmetric vibration of some chemisorbed species, such as OH groups at 1618 cm^{-1}, COOH species at 1623 cm^{-1} or HCO_3^- species at 1658 cm^{-1} resulting from the reaction of CO_2 with the surface OH groups.[12,30] The wide band from 1590 cm^{-1} to 1290 cm^{-1} was possibly assigned to stretching vibration of C=O or asymmetric stretching of O-C=O belonging to chemisorbed carbonate species (CO_3^{2-}).[12] After irradiation for 8 h, it was found that the intensities of chemisorbed species increased on the Ta_3N_5 while slightly decreased on the $LaTiO_2N$. This fact may imply that the chemisorbed species were important intermediates during CO_2 photoreduction. Notably, these intermediates, such as CO_3^{2-} species, were usually the result of CO_2 activation, thus boosting the CO_2 reduction kinetics. That is, the faster/slower consumption of the chemisorbed species would contribute to the higher/lower CO_2 reduction efficiency on $LaTiO_2N$ and Ta_3N_5, respectively. The new bands at 2920 and 2851 cm^{-1} belonging to CH_x^* species,[49] serving as an important intermediate for reduction of CO_2 to CH_4,[27] were only detected by FT-IR on $LaTiO_2N$ during the CO_2 conversion, further verifying that the high CH_4 selectivity on $LaTiO_2N$ was possibly a result of efficient CO_2 reduction *via* CH_x^* intermediates. The CO_3^{2-} species was also observed on Ta_3N_5 after the irradiation. And to promote the formation of CO_3^{2-} species by the modification of KOH (0.5 wt.%) on Ta_3N_5 surface, the CO_2 reduction efficiency (0.71 μmol/g for CO and 0.30 μmol/g for CH_4) enhanced significantly, while the CO selectivity (CH_4/CO=0.42) kept unchanged (**Fig. S6d, ESI†**). Similar results were observed for the MgO modified TiO_2 and KOH modified C_3N_4.[10,50] These evidences indicated that the product selectivity on both of Ta_3N_5 and $LaTiO_2N$ was not dependent on the formation of CO_3^{2-} species.

XPS analysis revealed that the -COOH at 288.4 eV and C=O species at 286.3 eV existed on the $LaTiO_2N$ and Ta_3N_5 surfaces (**Fig. 5c** and **5d**).[23,30] The absent CH_x^* species in XPS was highly possible for its low amount due to its fast reaction kinetics, as confirmed by the FT-IR analysis. During the irradiation, the formation of -COOH species on $LaTiO_2N$ is evidently faster than that on the Ta_3N_5. It was well known that the CO resulted mainly from dehydroxylation of -COOH species with the assitance of the photogenerated electrons and protons.[5,23] This evidence suggested that the the reaction kinetics for converting CO_2 to -COOH species were mainly responsible for the CO generation on Ta_3N_5 surface. The much lower amount of C=O species on $LaTiO_2N$ surface under irradiation, as indicated by the decreased peak intensity, demonstrated that the C=O species on $LaTiO_2N$ surface was rapidly consumed by the photoelectrons for the CH_4 formation. Indeed, the Ta_3N_5 with low CH_4 yields showed a little difference in concentration of C=O species before and after the irradiation. Hence, the possible reaction pathway of CO_2 reduction was proposed as $CO_2 \rightarrow COOH^* \rightarrow CO \rightarrow CH_x^* \rightarrow CH_4$. Our previous work demonstrated that the La as a basic site on porous $LaTiO_2N$ particles without exposure of specific facet

View Article Online
DOI: 10.1039/C8TA05339A

contributed to the CO_2 activation and the CH_4 selectivity.[30] The similar CH_4 selectivity on the $LaTiO_2N$ with dominant (002) surface probably meant that the CO_2 activation and product selectivity on $LaTiO_2N$ did not depend on the specific facets but still were dominated by La element. However, the performed CO_2 reduction experiment over the Ta_3N_5 without specific exposed crystal facet, which was prepared by nitriding Ta_2O_5 powders at 1123 K for 8 h under 500 mL/min NH_3, exhibited the main product of CH_4 with a CH_4/CO mole ratio of 1.95 (**Fig. S7a, ESI**†), confirming that the high CO selectivity was highly dependent on the exposed (020) facet of Ta_3N_5. Judging by the FT-IR and C 1s XPS analysis, the high CO selectivity of Ta_3N_5 with exposed (020) facet was probably related to the difficulty in hydrogenation of CO for generating CH_4 on the N-rich facet.

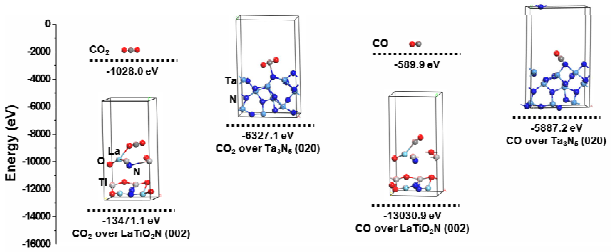

Fig. 6 The energies for CO_2 or CO adsorbed on $LaTiO_2N$ (002) and Ta_3N_5 (020) facets. The calculated energies for $LaTiO_2N$ (002) and Ta_3N_5 (020) facets were -12440.2 and -5297 eV, respectively.

Table 1. Adsorption energy, geometric parameter change before and after adsorption of CO_2 and CO over the surface of $LaTiO_2N$ (002) and Ta_3N_5 (020) facet.

	CO_2	CO_2 adsorption	
		Ta_3N_5 (020)	$LaTiO_2N$ (002)
E_{ads} [eV]	-	-2.1	-2.9
$d_{C\text{-}O}$ [Å]	1.151	1.178	1.179,1.188
∠O-C-O [°]	180	178.8	178.2
	CO	CO adsorption	
		Ta_3N_5 (020)	$LaTiO_2N$ (002)
E_{ads} [eV]	-	-0.3	-0.8
$d_{C\text{-}O}$ [Å]	1.129	1.157	1.166

To further explore the mechanism of the product selectivity, the surface models of $LaTiO_2N$ (002) and Ta_3N_5 (020) facet, the highly exposed facets by TEM observations, were built for calculations of adsorbed energies of CO_2 and CO by density functional theory (DFT). The adsorbed energy of an adsorbate on a given photocatalyst was calculated by the equation of $E_{ads} = E_{ads/pho} - E_{pho} - E_{adsorbate}$. Where, E_{ads} is adsorption energy. $E_{ads/pho}$, E_{pho} and $E_{adsorbate}$ are energy of adsorption system, energy of a photocatalyst and energy of an adsorbate, respectively. The calculated results were illustrated in **Fig. 6** and **Table 1**. The calculated results showed that the E_{ads} for CO_2 on Ta_3N_5 (020) surface was -2.1 eV, which was about 0.8 eV lower than that on $LaTiO_2N$ (002) facet (-2.9 eV). As can be seen, on the Ta_3N_5 (020) surface, the CO_2 was absorbed at N sites *via* interactions between C and N atoms because the stable terminal facet was consisted of N atom layer. In general, the CO_2 was inclined to absorb onto the metal atom sites because of their low electronegativity.[4,29] Similarly, on the surface of $LaTiO_2N$, the CO_2 with a tilted structure was absorbed at La sites by contacting with O atoms of CO_2. As well demonstrated in our previous report, the La sites were served as basic sites for effectively catalyzing CO_2 into CH_4.[30] Similarly, the adsorbed CO_2 on $LaTiO_2N$ was also activated, as demonstrated by the increased C-O bonding length (from 1.151 Å to 1.179/1.188 Å) and decreased O-C-O bonding angle (from 180° to 178.2°). In contrast, the CO_2 on Ta_3N_5 surface was adsorbed with slightly shorter C-O bonding length (1.178 Å) and wider O-C-O bonding angle (178.8°). This may induce the faster and lower formation rate for -COOH species by CO_2 activation on $LaTiO_2N$ and Ta_3N_5 surface, respectively.

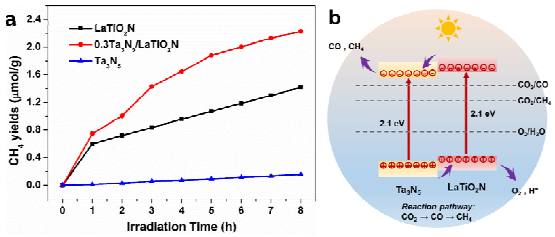

Fig. 7 (a) The CH_4 yields over $LaTiO_2N$, Ta_3N_5, and $0.3Ta_3N_5/LaTiO_2N$ using CO as carbon source under visible light. b) The possible CO_2 reduction mechanism for $Ta_3N_5/LaTiO_2N$.

Obviously, the calculated results showed that the E_{ads} for CO on Ta_3N_5 (020) surface (-0.33 eV) was about 0.5 eV lower than that on $LaTiO_2N$ (002) facet (-0.83 eV). The strong CO adsorption on $LaTiO_2N$ may provide the possibility to covert the CO into CH_4 by subsequent hydrogenation. In another word, the desorption of CO on Ta_3N_5 (020) facet was much easier than that on $LaTiO_2N$ surface. As expected, the (023) surface model of Ta_3N_5 was built, an exposed facet for the Ta_3N_5 prepared from direct nitridation of Ta_2O_5 particles, as observed by TEM. It was found that the (023) facet with relatively rich Ta atoms showed a much higher CO capture ability (-2.7 eV) and the CO was indeed adsorbed at Ta site (**Fig. S7a, ESI**†). After stable adsorption, the increase of C-O bonding length of CO (1.129 Å) was obviously larger on the surface of $LaTiO_2N$ (1.166 Å) than Ta_3N_5 (1.157 Å). This result indicated that CO activation was easier to occur on the La sites on $LaTiO_2N$ by comparing to the N sites of Ta_3N_5, thus boosting the CH_4 formation. A photocatalytic test was carried out to check the photocatalytic reaction of CO, performing under the CO (5% mole)+argon mixed gases. Indeed, in the presence of H_2O, the $LaTiO_2N$ could rapidly convert the CO into CH_4 (1.42 μmol/g for 8 h) **(Fig. 7a)**, truly confirming that the CO could be further converted into CH_4. In contrast, a much low conversion efficiency was observed for the Ta_3N_5 (0.16 μmol/g for 8

View Article Online
DOI: 10.1039/C8TA05339A

h), confirming its poor ability to convert CO into CH_4. For the $0.3Ta_3N_5/LaTiO_2N$, due to the high charge separation, an improved CH_4 yield was also obtained (2.22 μmol/g for 8 h). These results prove that the product selectivity of CO_2 reduction is dependent on the surface chemistry of Ta_3N_5 and $LaTiO_2N$.

On the basis of the above results, the product selectivity for the CO_2 reduction over $Ta_3N_5/LaTiO_2N$ heterojunction was proposed in **Fig. 7b.** Under the visible light, the lower CB and VB positions of Ta_3N_5 induce directional electron flow from CB of $LaTiO_2N$ to CB of Ta_3N_5 and reversed hole transfer between their VBs. The high CO selectivity was achieved on (020) surface of Ta_3N_5 due to the poor ability in converting -COOH intermediate and the weak CO adsorption. Meanwhile, the high CH_4 selectivity produced on the $LaTiO_2N$ due to the strong CO adsorption and efficiently activating carbon-based precursors to CH_x^*, probably on the La base metal sites.

Conclusions

In summary, using the $LaTiO_2N$ with exposure of (002) facet and Ta_3N_5 with dominant (020) facet as model photocatalysts, we have showed that the product selectivity for CO_2 reduction on photocatalyst is strongly associated to the kinetics of molecule activation and intermediate conversion. The (020) surface of Ta_3N_5 terminated by N atoms exhibits the poor ability in converting -COOH intermediate and the weak CO adsorption, thus inducing the high CO selectivity. The high CH_4 selectivity on the $LaTiO_2N$ is not facet-dependent, more likely to be dominated by La base metal sites to efficiently activate carbon-based precursors to CH_x^*. Our findings indicated that the surface chemistry of catalyst was a significant factor for the selective product formation of the photocatalytic CO_2 reduction.

Conflicts of interest

There are no conflicts to declare.

Acknowledgements

This work was supported primarily by the National Basic Research Program of China (2013CB632404), the National Natural Science Foundation of China (51572121, 21603098 and 21633004), the Natural Science Foundation of Jiangsu Province (BK20151265, BK20151383 and BK20150580), the Fundamental Research Funds for the Central Universities (021314380133 and 021314380084), the Postdoctoral Science Foundation of China (2017M611784), Six talent peaks project in Jiangsu Province (YY-013) and the program B for outstanding PhD candidate of Nanjing University (201702B084).

References

1 J. Ran, M. Jaroniec and S. Z. Qiao, *Adv. Mater.*, 2018, **30**, 1704649.
2 Y. Zheng, W. Q. Zhang, Y. F. Li, J. Chen, B. Yu, J. C. Wang, L. Zhang and J. J. Zhang, *Nano Energy*, 2017, **40**, 512.
3 J. H. Wu, Y. Huang, W. Ye and Y. G. Li, *Adv. Sci.*, 2017, **4**, 1700194.
4 W. G. Tu, Y. Zhou and Z. G. Zou, *Adv. Mater.*, 2014, **26**, 4607.
5 S. N. Habisreutinger, L. Schmidt-Mende and J. K. Stolarczyk, *Angew. Chem. Int. Ed.*, 2013, **52**, 7372.
6 L. J. Liu, H. L. Zhao, J. M. Andino and Y. Li, *ACS Catal.*, 2012, **2**, 1817.
7 Z. F. Jiang, W. M. Wan, H. M. Li, S. Q. Yuan, H. J. Zhao and P. K. Wong, *Adv. Mater.*, 2018, **30**, 1706108.
8 S. C. Yan, J. J. Wang, H. L. Gao, N. Y. Wang, H. Yu, Z. S. Li, Y. Zhou and Z. G. Zou, *Adv. Funct. Mater.*, 2013, **23**, 758.
9 Q. Liu, Y. Zhou, J. H. Kou, X. Y. Chen, Z. P. Tian, J. Gao, S. C. Yan and Z. G. Zou, *J. Am. Chem. Soc.*, 2010, **132**, 14385.
10 S. J. Xie, Y. Wang, Q. H. Zhang, W. Q. Fan, W. P. Deng and Y. Wang, *Chem. Commun.*, 2013, **49**, 2451.
11 W. N. Wang, W. J. An, B. Ramalingam, S. Mukherjee, D. M. Niedzwiedzki, S. Gangopadhywy and P. Biswas, *J. Am. Chem. Soc.*, 2012, **134**, 11276.
12 X. G. Meng, S. X. Ouyang, T. Kako, P. Li, Q. Yu, T. Wang and J. H. Ye, *Chem. Commun.*, 2014, **50**, 11517.
13 S. Neaţu, J. A. Maciá-Agulló, P. Concepción and H. Garcia, *J. Am. Chem. Soc.*, 2014, **136**, 15969.
14 Q. Q. Lang, Y. J. Yang, Y. Z. Zhu, W. L. Hu, W. Y. Jiang, S. X. Zhong, P. J. Gong, B. T. Teng, L. H. Zhao and S. Bai, *J. Mate. Chem. A*, 2017, **5**, 6686.
15 S. C. Yan, L. J. Wan, Z. S. Li and Z. G. Zou, *Chem. Commun.*, 2011, **47**, 5632.
16 J. G. Yu, J. X. Low, W. Xiao, P. Zhou and M. Jaroniec, *J. Am. Chem. Soc.*, 2014, **136**, 8839.
17 J. Mao, T. Y. Peng, X. H. Zhang, K. Li and L. Zan, *Catal. Commun.*, 2012, **28**, 38.
18 Y. Y. Liu, B. B. Huang, Y. Dai, X. Y. Zhang, X. Y. Qin, M. H. Jiang and M. Whangbo, *Catal. Commun.*, 2009, **11**, 210.
19 S. M. Wang, Y. Guan, L. Lu, Z. Shi, S. C. Yan and Z. G. Zou, *Appl. Catal. B Environ.*, 2018, **224**, 10.
20 S. B. Wang, B. Y. Guan, Y. Lu, X. Wen and D. Lou, *J. Am. Chem. Soc.*, 2017, **139**, 17305.
21 J. G. Hou, S. Y. Cao, Y. Z. Wu, F. Liang, L. Ye, Z. S. Lin and L. C. Sun, *Nano Energy*, 2016, **30**, 59.
22 M. L. Li, L. X. Zhang, M. Y. Wu, Y. Y. Du, X. Q. Fan, M. Wang, L. L. Zhang, Q. L. Kong and J. L. Shi, *Nano Energy*, 2016, **19**, 145.
23 J. Rosen, G. S. Hutchings, Q. Lu, S. Rivera, Y. Zhou, D. G. Vlachos and F. Jiao, *ACS Catal.*, 2015, **5**, 4293.
24 W. L. Zhu, Y. J. Zhang, H. Y. Zhang, H. F. Lv, Q. Li, R. Michalsky, A. A. Peterson and S. H. Sun, *J. Am. Chem. Soc.*, 2014, **136**, 16132.
25 D. D. Zhu, J. L. Liu and S. Z. Qiao, *Adv. Mater.*, 2016, **28**, 3423.
26 S. Kattel, P. Liu and J. G. Chen, *J. Am. Chem. Soc.*, 2017, **139**, 9739.
27 Y. F. Ji and Y. Luo, *J. Am. Chem. Soc.*, 2016, **138**, 15896.
28 A. E. Maegli, S. Pokrant, T. Hisatomi, M. Trottmann, K. Domen and A. Weidenkaff, *J. Phys. Chem. C*, 2013, **118**, 16344.
29 J. C. Matsubu and V. N. Yang, *J. Am. Chem. Soc.*, 2015, **137**, 3076.
30 L. Lu, B. Wang, S. M. Wang, Z. Shi, S. C. Yan and Z. G. Zou, *Adv. Funct. Mater.*, 2017, **27**, 1702447.
31 R. B. Singh, H. Matsuzaki, Y. Suzuki, K. Seki, T. Minegishi, T. Hisatomi, K. Domen and A. Furube, *J. Am. Chem. Soc.*, 2014, **136**, 17324.
32 M. Sluban, P. Umek, Z. Jagličic, J. Buh, P. Smitek, A. Mrzel, C. Bittencourt, M. H. Delville, D. Mihailovic and D. Arcon, *ACS Nano*, 2015, **9**, 10133.
33 Y. Qi, S. S. Chen, M. R. Li, Q. Ding, Z. Li, J. Y. Cui, B. B. Dong, F. X. Zhang and C. Li, *Chem. Sci.*, 2017, **8**, 437.
34 F. Zuo, L. Wang, T. Wu, Z. Zhang, D. Borchardt and P. Feng, *J. Am. Chem. Soc.*, 2010, **132**, 11856.
35 M. Batzill, E. H. Morales and U. Diebold, *Phys. Rev. Lett.*, 2006, **96**, 026103.
36 Y. G. Li, H. Song, F. Li, X. Li, Z. R. Lou, Z. Z. Ye and L. P. Zhu, *Nano Energy*, 2016, **19**, 437.

View Article Online
DOI: 10.1039/C8TA05339A

37 M. Matsukawa, R. Ishikawa, T. Hisatomi, Y. Moriya, N. Shibata, J. Kubota and K. Domen, *Nano Lett.*, 2014, **14**, 1038.
38 X. B. Chen, L. Liu, Y. Peter and S. S. Mao, *Science*, 2011, **331**, 746.
39 G. Liu, L. C. Yin, J. Q. Wang, P. Niu, C. Zhen, Y. P. Xie and H. M. Cheng, *Energy Environ. Sci.*, 2012, **5**, 9603.
40 G. Liu, J. Pan, L. C. Yin, J. T. S. Irvine, F. Li, J. Tan, P. Wormald and H. M. Cheng, *Adv. Funct. Mater.*, 2012, **22**, 3233.
41 X. X. Xu, C. Randorn, P. Efstathiou and J. T. S. Irvine, *Nat. Mater.*, 2012, **11**, 595.
42 K. K. Banger, Y. Yamashita, K. Mori, R. L. Peterson, T. Leedham, J. Rickard, H. Sirringhaus, *Nat. Mater.*, 2011, **10**, 45.
43 Y. G. Li, X. B. Cheng, X. Y. Ruan, H. Song, Z. R. Lou, Z. Z. Ye and L. P. Zhu, *Nano Energy*, 2015, **12**, 775.
44 Y. M. He, J. E. Thorne, C. H. Wu, P. Y. Ma, C. Du, Q. Dong, J. H. Guo and D. W. Wang, *Chem*, 2016, **1**, 640.
45 L. Wang, X. M. Zhou, N. T. Nguyen, I. Hwang and P. Schmuki, *Adv. Mater.*, 2016, **28**, 2432.
46 S. J. A. Moniz, S. A. Shevlin, D. J. Martin, Z. X. Guo and J. W. Tang, *Energy Environ. Sci.*, 2015, **8**, 731.
47 J. J. Wang, T. Fang, L. Zhang, J. Y. Feng, Z. S. Li and Z. G. Zou, *J. Catal.*, 2014, **309**, 291.
48 M. Tahir and N. A. S. Amin, *Appl. Catal. B Environ.*, 2015, **162**, 98.
49 W. Yu, D. Xu and T. Peng, *J. Mater. Chem. A*, 2015, **3**, 19936.
50 Z. X. Sun, J. M. T. A. Fischer, Q. Li, J. Hu, Q. J. Tang, H. Q. Wang, Z. B. Wu, M. Hankel, D. J. Searles and L. Z. Wang, *Appl. Catal. B Environ.*, 2017, **216**, 146.

TOC

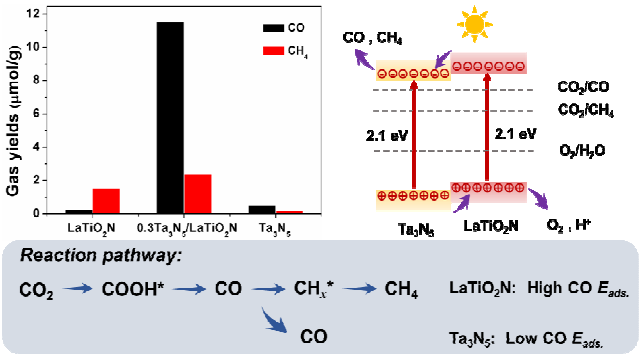

The product selection for CO_2 reduction depends on the surface chemistry of Ta_3N_5 and $LaTiO_2N$ photocatalyst.